RSC Advances

ROYAL SOCIETY OF CHEMISTRY

www.rsc.org/advances

Journal Name

RSCPublishing

ARTICLE

Photoluminescence and photocatalytic activity of monodispersed colloidal "ligand free Ln^{3+}-doped $PbMoO_4$ nanocrystals"

Cite this: DOI: 10.1039/x0xx00000x

Received 00th January 2012,
Accepted 00th January 2012

DOI: 10.1039/x0xx00000x

www.rsc.org/

Sagar Ganguli,[a] Chanchal Hazra,[a] Tuhin Samanta [a] and Venkataramanan Mahalingam[a*]

In this article, we have shown a synthetic strategy to prepare ligand-free colloidal Eu^{3+}-doped $PbMoO_4$ nanocrystals that form a stable dispersion in polar solvents. The surface of the nanocrystals is designed to have excess residual ions (Pb^{2+} or MoO_4^{2-}) compared to the counter-ionic species, thereby providing a partially charged nanocrystal surface. These charged nanocrystal surfaces cause electrostatic repulsion, providing colloidal stability in polar solvents. Microscopic measurements suggest the formation of spherical shaped nanocrystals with an average size of 10 nm. Upon UV excitation, aqueous dispersions of the Eu^{3+}-doped $PbMoO_4$ nanocrystals display intense red emission characteristic of Eu^{3+} ions. Furthermore, under UV irradiation, the nanocrystals exhibit strong photocatalytic activity, which is verified from the degradation of Rhodamine B dye. The Rhodamine B dye is significantly degraded by ~70% under UV illumination within 3h at pH 5.5. The strong luminescence efficiency and photocatalytic activity make the water dispersible Ln^{3+}-doped $PbMoO_4$ nanocrystals a potential material for dual applications like luminescent and photocatalyst.

1. Introduction

Lanthanide ions (Ln^{3+}) exhibit interesting optical properties arising from their sharp intra 4*f*-4*f* transitions.[1,2] These intra 4*f* transitions are partially forbidden leading to quite narrow luminescence emissions with longer lifetime ranging from µs to ms.[3-5] Ln^{3+}-doped nanocrystals (NCs) have attracted huge interests in the recent years owing to their unique optical properties which make them potential candidates in laser materials, colour displays, optoelectronic devices, photocatalysis, solar cells, biosensors, just to name a few.[6-11] Among various host matrices available for Ln^{3+} ions, oxides are widely studied due to their high robustness along with chemical and thermal stabilities.[12,13] However, their synthesis generally involves high temperatures and long reaction times. Moreover, the resulting products are generally solids with low dispersibility in various solvents. To envision the full potential of the Ln^{3+}-doped materials for various applications, synthesis of colloidal NCs is important.

Synthesis of colloidal Ln^{3+}-doped NCs are generally achieved using capping ligands with various functional groups like COOH, PO_4^{2-}, SO_4^{2-} etc.[14] The ligands play a dual role such as controlling the size as well as enhancing the dispersibility of the NCs in various solvents. However, the presence of strong vibrational modes of the ligands such as C-H, O-H or N-H can in principle enhance the non-radiative relaxation of excited Ln^{3+} ions leading to reduction in luminescence efficiency. Moreover, for photocatalytic applications, the capping ligands act as an inhibitor as they reduce the chances of electron and hole transfers from the catalyst to oxygen or substrate. To overcome these problems, a post synthesis modification of the nanocrystal surface is generally performed to get rid of the insulating ligands prior to their use in electronic and optoelectronic devices.[15-20] This process could be tedious as the ligand removal may lead to particle coagulation. An alternative to this technique is to prepare partially charged surfaces using non-stoichiometric amount of precursors. The residual charge on the NCs' surface will assist to prepare stable colloidal solutions in polar solvents (by electrostatic interaction). Similar concept of colloidal stabilization was first reported more than a century ago when I^- ions were employed to stabilize AgI colloids.[21] Recently, Nag *et al.* have reported the synthesis of ligand free metal sulfide NCs following the same approach.[22] Addition of non-stoichiometric amount of precursors generated a nanocrystal surface bearing excess of sulfide (CdS_{1+x}) ions leading to negatively charged nanocrystal surface. Most of the studies on ligand free nanocrystal synthesis were restricted to semiconductors. However, such studies are not much explored to prepare other NCs, particularly Ln^{3+}-doped oxide NCs which can be challenging. For example, Rao *et al.* have extensively investigated the photocatalytic activity of electron rich and electron deficient TiO_2- graphene composites without ligands. They have correlated the results with the nature of interaction between the composites and adsorbed dye molecules.[23] The same group has also investigated the role of

defects on laser excited photoluminescence of various ZnO nanostructures.[24] Our idea is to develop synthetic routes to prepare ligand free oxide NCs which can be used for luminescent as well as photocatalytic applications. We have chosen $PbMoO_4$ for this purpose.

Among the various molybdates, $PbMoO_4$ has drawn much attention due to their wide use in optical instrument engineering, photoconductivity, etc.[25-26] The lower band gap energy of $PbMoO_4$ nanomaterials compared to other metal molybdates make them potential candidate for UV light induced photocatalytic activity and water splitting applications.[27] There are quite a few reports available on the synthesis of $PbMoO_4$ via high temperature solid-state methods.[28] In recent years, few solution-phase routes have been employed to synthesize $PbMoO_4$ nanomaterials and microcrystals. For example, Uresti et al. have investigated the photocatalytic activity of $PbMoO_4$ NCs prepared through microwave procedure. The material prepared through this method shows better photocatalytic activity than the one prepared from solid state method. The same group investigated the effect of pH on the photocatalytic activity of $PbMoO_4$ NCs. The as synthesized photocatalyst achieved degradation of 30% for Rhodamine B (RhB) dye at pH 5.5, while at pH 4, dye degradation was recorded close to 100%.[29] Shen et al. have reported a facile CTAB-assisted hydrothermal process to prepare $PbMoO_4$ microcrystals with preferentially exposed (001) facets.[30]

In this article, we report the synthesis of water dispersible ligand free Eu^{3+}-doped $PbMoO_4$ NCs using microwave procedure for the first time. The water dispersibility is achieved through preparation of non-stoichiometric surfaces. Excess residual ions on the surface of the nanocrystal cause repulsive interaction between the NCs, thereby providing colloidal stability. These NCs show intense luminescence signals in water. Furthermore, the NCs display strong photocatalytic activity, which is verified through the degradation of RhB dye. We observed ~70% degradation of RhB under UV illumination at pH 5.5. The intense luminescence together with photocatalytic activity of the Eu^{3+}-doped $PbMoO_4$ NCs make them potential materials for dual applications.

2. Experimental

2.1 Materials: Eu_2O_3 and Rhodamine B AR were purchased from Sigma Aldrich and LobaChemie, respectively. Sodium Molybdate Dihydrate [$Na_2MoO_4{\cdot}2H_2O$], Lead Nitrate [$Pb(NO_3)_2$], 1 (M) HNO_3 (70% pure) and Formamide were purchased from Merck. All the chemicals were used without further purification.

2.2 Synthesis: Eu^{3+} doped $PbMoO_4$ NCs were prepared by microwave method. Briefly, 0.025 mmol of Eu_2O_3 was stirred with concentrated HNO_3 and heated at 95°C to produce $Eu(NO_3)_3$. Formamide was added to $Eu(NO_3)_3$ and stirred for 10 minutes to make a transparent solution. This solution was then added to 0.95 mmol $Pb(NO_3)_2$ followed by further addition of 5 ml formamide. To this mixture, a solution containing 1 mmol of Na_2MoO_4 / 5 ml formamide has been added slowly followed by 30 min of vigorous stirring. The resultant solution was subsequently transferred into a 30 ml glass vial capped tightly with silicone septum. The sealed vial was kept in the microwave reactor (Anton Paar Monowave 300) and the reaction was carried out for 10 min at a temperature of 150 °C. Subsequently, the reaction system was allowed to cool down to room temperature. The product was collected by centrifugation and washed thrice with deionized water and ethanol to remove any unreacted reactants. The product was then dried under vacuum. The same protocol was followed to prepare two more samples, one using 0.021 mmol Eu_2O_3, 0.80 mmol $Pb(NO_3)_2$ and 1 mmol of Na_2MoO_4, while the other contained 0.029 mmol Eu_2O_3, 1.10 mmol $Pb(NO_3)_2$ and 1 mmol of Na_2MoO_4. NCs synthesized from 0.80 mmol $Pb(NO_3)_2$, 0.95 mmol $Pb(NO_3)_2$ and 1.10 mmol $Pb(NO_3)_2$ have been designated as Pb80, Pb95 and Pb110 respectively in all future references. For comparative studies, undoped $PbMoO_4$ and La^{3+} (optically silent) doped $PbMoO_4$ were also prepared using the same protocol.

2.3 Characterisation The XRD patterns were collected using a Rigaku-SmartLab diffractometer attached with a D/tex ultra detector and Cu Kα source operating at 35 mA and 70 kV. The scan range was set from 10-60° 2θ with a step size of 0.02° and a count time of 2 s. The samples were well powdered and spreaded evenly on a quartz slide. Field emission scanning electron microscopy (FE-SEM) images were taken on a SUPRA 55-VP instrument with patented GEMINI column technology. Prior to loading the samples into the chamber, they were coated with a thin film of gold-palladium in order to avoid charging effects. DLS measurements were carried out in a Malvern Zetasizer Nano equipped with a 4.0 mW He–Ne laser operating at λ= 633 nm. Thermogravimetric analysis (TGA) was performed using a Mettler Toledo TGA 851 instrument under N_2 atmosphere at a heating rate of 10° min^{-1}. The PL spectra were measured on a Horiba Jobin Yvon spectrometer equipped with a 450 W Xe lamp. The excitation and emission light were dispersed using a Czerny-Turner monochromator with an optical resolution of 1 nm. The emitted photons were detected using a Hamamatsu R928 detector. The output signal was recorded using a computer. The PL lifetime measurements were performed with a Horiba Jobin Yvon Fluorolog CP machine equipped with a pulsed Xe source operating at 25 W. Diffused reflectance spectroscopy measurements of the samples were done using Jasco V670.

The photocatalytic activity of all three $PbMoO_4$ NCs were evaluated by degradation of RhB dye under UV irradiation using a Xe lamp (Newport, Standford) with 140 W power (70 mA). In each experiment, 50 mg of photocatalyst was added into 50 ml of RhB solution with a concentration of $5X10^{-5}$ mol L^{-1}. Prior to irradiation, the suspensions were stirred in dark for 30 min to reach adsorption-desorption equilibrium, following which, the dispersions were exposed to radiation using a solar simulator with continuous magnetic stirring. At regular irradiation time interval, a 3 ml aliquot of the suspension was collected, and the slurry samples, including the photocatalyst and RhB solution, were centrifuged (6000 rpm, 5 min) to remove the photocatalyst particles in order to assess the rate of decolourization and degradation photometrically. The solutions were analyzed by a Hitachi UV-4100 UV-Vis-NIR spectrophotometer, and the characteristic absorption of RhB at 554 nm was used to monitor the photocatalytic degradation. For comparative studies, photocatalytic experiments were carried out with undoped $PbMoO_4$, La^{3+} doped $PbMoO_4$ and TiO_2 (P25) following the same procedure. All measurements were carried out at room temperature.

3. Results and discussion

The ligand free colloidal Eu^{3+}-doped $PbMoO_4$ NCs were synthesized using microwave procedure for the first time. The reason for choosing Eu^{3+} ions is due to its strong luminescence with lifetimes in the millisecond range. In addition, they are useful dopants as optical probes to provide information about the local crystalline environment around the Ln^{3+} ions.[31] Powder XRD patterns of all the samples (Pb80, Pb95, Pb110, undoped $PbMoO_4$ and La^{3+} doped $PbMoO_4$) are displayed in Fig. 1. The patterns confirm the formation of the tetragonal phase (wulfenite) $PbMoO_4$, which match well with the standard pattern of $PbMoO_4$ (PDF Card No.- 01-089-8706) with a space group I41/a(88). The sharp patterns clearly imply the formation of highly crystalline materials, which are prerequisite for intense emission from Eu^{3+}-doped materials. The absence of any additional peak suggests that $PbMoO_4$ NCs with high phase purity can be easily obtained through the microwave synthetic method. The lattice parameters (a and c) for Pb80 NCs are 5.4287 Å and 12.0921 Å, while the corresponding values for Pb95 and Pb110 NCs are 5.4233 Å, 12.1067 Å and 5.4213 Å, 12.1136 Å, respectively. For undoped $PbMoO_4$ and La^{3+} doped $PbMoO_4$, the lattice parameters were found to be 5.4224 Å, 12.1063 Å and 5.4229 Å, 12.1077 Å respectively. These values closely match with that of the reported values.[32]

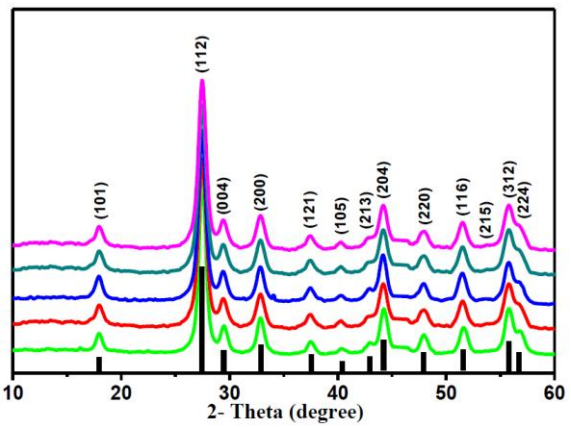

Fig. 1. XRD patterns of $PbMoO_4$ nanocrystals: (green) Pb80, (red) Pb95, (blue) Pb110, (cyan) undoped $PbMoO_4$, (pink) La^{3+} doped $PbMoO_4$ and (black) the standard pattern.

The average crystallite sizes of all Eu^{3+}-doped $PbMoO_4$ NCs were calculated using Debye-Scherrer equation, $D = 0.9\lambda/(\beta \cos\theta)$, where D denotes the average crystallite size, λ (= 1.5418 Å) is the wavelength of incident X-ray, β is the corrected full width half-maxima (FWHM) and θ is the diffraction angle for the (hkl) plane. The crystallite sizes obtained for Pb80, Pb95, Pb110, undoped $PbMoO_4$ and La^{3+} doped $PbMoO_4$ samples are 11 nm, 9 nm, 10.4 nm, 8.8 nm and 9.2 nm, respectively. The tetragonal structure of $PbMoO_4$ NCs is also evident from the basic unit cell crystal structure shown in Fig. 2a, which was obtained using VESTA program.[33] In the $PbMoO_4$ crystal structure, the Pb^{2+} ions occupy octahedral positions and Mo^{6+} atoms are in the centre of slightly distorted tetrahedra MoO_4^{2-}.

FE-SEM images revealed formation of spherical NCs in all three cases. However, Pb80 and Pb110 form highly monodisperse solutions while Pb95 mostly stays in aggregated form. Fig. 2b suggests the formation of spherical NCs with an average size of 13 nm for Pb80 sample. In the case of Pb95 and Pb110 samples, the corresponding values are 9 and 12 nm, respectively (shown in Fig. 2c and 2d). The high monodispersity in the size is further substantiated by the narrow distribution obtained with DLS measurements in water (Fig. S1). The hydrodynamic size of the NCs obtained from the DLS measurements are about 20 and 18 nm for Pb80 and Pb110 NCs, respectively and thereby supports the SEM results.

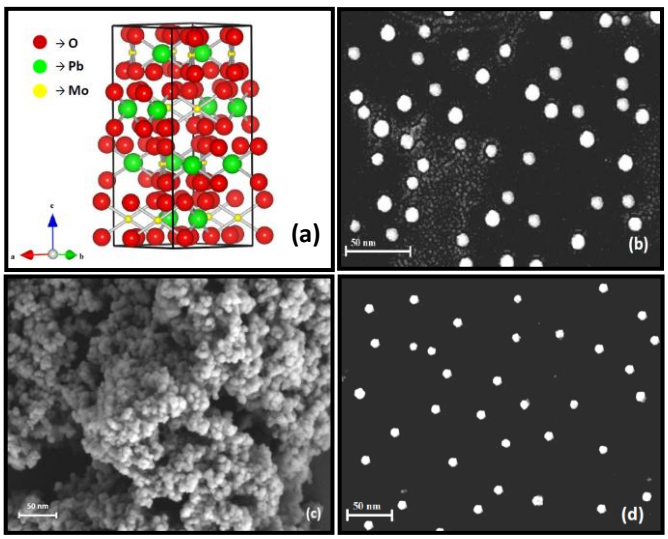

Fig. 2. (a) Tetragonal crystal structure of Eu^{3+} doped $PbMoO_4$ NCs created using VESTA program. SEM images of (b) Pb80, (c) Pb95 and (d) Pb110, indicating spherical morphology.

To check the colloidal stability of the NCs in polar solvents, 5 mg of each sample was added to 5 ml of formamide (dielectric constant, ε=106) separately and sonicated for one hour. The resulting mixtures were left undisturbed to investigate their colloidal stability. The digital images (shown in Fig. 4a) reveal that, within one hour Pb95 NCs settle down, as a result of which, the letters in the back side of the vial becomes visible through the solvent. The other two samples (Pb80 and Pb110) show good colloidal stability. Similar trend in colloidal stability was also observed when the NCs were dispersed in water (ε=80).

It is interesting to note that addition of non-stoichiometric amount of precursors (e.g. Pb^{2+} and MoO_4^{2-}) gives rise to the formation of charged nanocrystal surface. The presence of non- stoichiometric amounts of Pb^{2+} and MoO_4^{2-} in Pb80 and Pb110 were verified from EDS analysis (shown in Fig. S2). In case of Pb80, as the atomic percentage of MoO_4^{2-} is more than that of Pb^{2+} (shown in Fig. S2a), a negatively charged surface is generated, which is experimentally verified by a negative zeta potential value of -20 mV. Similarly, for Pb110, excess atomic percentage of Pb^{2+} than MoO_4^{2-} (shown in Fig. S2c) produces a positively charged surface, which is further characterised by a positive zeta potential value of +18 mV. Similar results of lower colloidal stability for positively charged surface than the negatively charged ones was reported for CdS NCs.[22] The atomic percentage of both Pb^{2+} and MoO_4^{2-} are almost same in Pb95 (shown in Fig. S2b) and as a result, its zeta potential value was found to be -0.10 mV. The zeta potential measurements for all the samples are shown in Fig. S3.

The ligand free nature of the $PbMoO_4$ NCs was verified by performing TGA and FTIR analysis (shown in Fig. S4 and S5, respectively). Upon heating, $PbMoO_4$ NCs lose less than 3% weight upto 500^{O}C temperature. We believe this negligible weight loss is due to the evaporation of residual formamide which was used as solvent in the microwave procedure. IR spectra of all three NCs show peaks near 1630, 1390 and 570 cm^{-1}, which belong to C=O stretching, C-H bending and torsion, respectively of formamide molecule. This indicates that formamide is indeed present in all three samples. However, the peaks of formamide are very weak in comparison to $PbMoO_4$ peaks. This along with TGA data confirm that very small amount of formamide is likely present in the products. Very small shifts of formamide peaks in the NCs suggest that they are loosely bound on the nanoparticle surface. These results indicate that formamide is very unlikely to act as capping ligands to make the NCs dispersible.[22]

Optical investigations of ligand free colloidal Eu^{3+}-doped $PbMoO_4$ NCs show some interesting characteristics. Upon UV (394nm) excitation, aqueous dispersion of all three samples show strong emission near 614 nm (as shown in Fig. 3a) which is assigned to $^5D_0 \rightarrow {}^7F_2$ transition. In addition to this strong emission at 614 nm, relatively less intense emission peaks are observed at 590, 650 and 700 nm, which are ascribed to $^5D_0 \rightarrow {}^7F_1$, $^5D_0 \rightarrow {}^7F_3$ and $^5D_0 \rightarrow {}^7F_4$ transitions, respectively. A scheme showing the origin of photoluminescence and the energy levels of Eu^{3+} is shown in Fig. 3b. The $^5D_0 \rightarrow {}^7F_1$ (590 nm) transition is magnetic-dipole transition whereas the $^5D_0 \rightarrow {}^7F_2$ (614 nm) is a hypersensitive electric-dipole transition whose intensity depends on the local crystalline environment around the Eu^{3+} ions in the host lattice. An intense $^5D_0 \rightarrow {}^7F_2$ transition generally arises when the emitting Eu^{3+} ions are present in the site of low symmetry environment. However, in $PbMoO_4$ lattice, both Pb^{2+} and Mo^{2+} have S_4 point symmetry possessing an inversion centre. This suggests weaker emission intensity for the $^5D_0 \rightarrow {}^7F_2$ transition. The observed strong emission might be due to the presence of some defects or disorders, which ultimately leads to the distortion in the symmetry sites where the Eu^{3+} ions occupy in the host lattice.[34] Moreover, we believe that polarization effect, which alters the crystal field strength as well as affects the transition probabilities, may be responsible for such observation.[35] Similar luminescence observations were reported in $REPO_4$: Ln^{3+} (RE = Y, La, Gd; Ln^{3+} = Eu^{3+}, Dy^{3+}, Tb^{3+}) phosphors.[36-37]

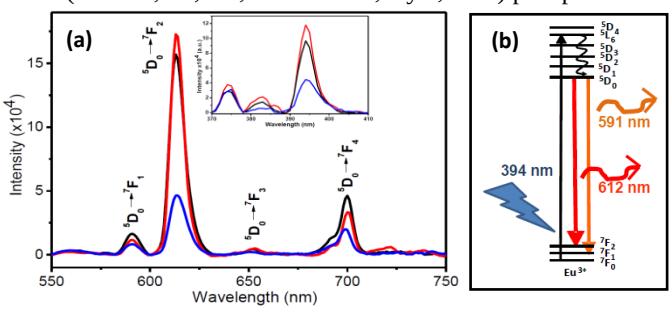

Fig. 3. (a) Emission spectra from Eu^{3+} ions doped in Pb80 (red), Pb95 (black) and Pb110 (blue) nanocrystals dispersed in water by 394 nm excitation. The inset shows the relative excitation spectra of the three samples recorded by monitoring the emission intensity at 612 nm. (b) Scheme depicting the origin of photoluminescence from Eu^{3+} doped $PbMoO_4$ nanocrystals.

It is interesting to note that the luminescence intensity of Eu^{3+} ions in Pb110 is lower than that of other two samples (Pb80 and Pb95). We emphasize that the difference in the emission intensity between the three NCs is not due to their difference in colloidal stability and size as Pb110, showing the lowest intensity, has higher colloidal stability as well as larger size than Pb95. The reason might be explained by considering that Eu^{3+} ions are not as good a candidate as Pb^{2+} ions for the matrix and as a result, all Eu^{3+} ions are not able to get doped into the host matrix in the presence of excess Pb^{2+} ions. Hence, it is relatively much more difficult for the Eu^{3+} ions to get doped into the Pb110 matrix during synthesis since, statistically, the ratio of Pb^{2+} to MoO_4^{2-} is more in the case of Pb110 compared to Pb95 and Pb80. More Eu^{3+} doping in the case of Pb80 and Pb95 compared to Pb110 results in relatively higher luminescence intensity for Pb80 and Pb95 than Pb110. EDS analysis (Fig. S2) of all three samples supports the aforementioned explanation. For Pb80 and Pb95, the atomic percentage of Eu^{3+} with respect to Pb^{2+} is almost 5%, while it is only about 2% for Pb110.

Time dependent luminescence intensity studies of all three NCs dispersed in water were further performed to evaluate their relative colloidal stabilities. The luminescence intensity of Eu^{3+} in Pb95 decreases rapidly with time (Fig. 4c). However, the observed decrease in the luminescence intensity for Pb80 and Pb110 NCs, is only 10% and 18%, respectively (after 180 minutes) suggesting the strong colloidal stability of these NCs (Fig. 4b and 4d, respectively). The steep decrease in the luminescence intensity for Pb95 suggests rapid settling down of the NCs.

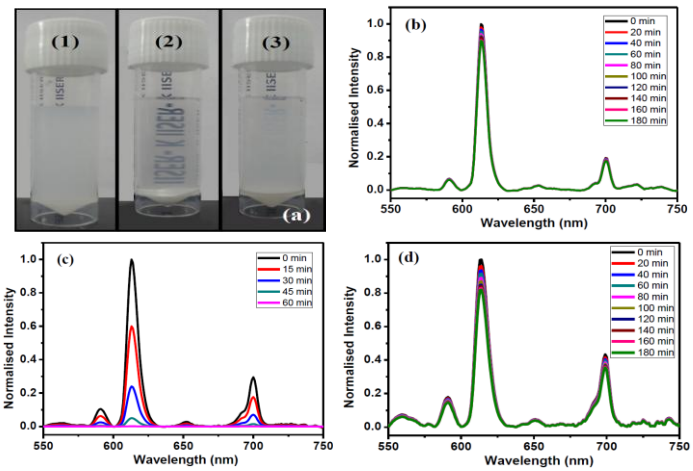

Fig. 4. (a) Digital images showing the relative stability of NC dispersions in formamide (ε=106) (The samples were left undisturbed for one hour after 1 h sonication) (1) Pb80, (2) Pb95 and (3) Pb110. Time dependent luminescence intensity studies of Eu^{3+}-doped $PbMoO_4$ NCs for determination of colloidal stability: (b) Pb80, (c) Pb95 and (d) Pb110.

The luminescence lifetime of the $^5D_0$ state of Eu^{3+} ions in Pb80, Pb95 and Pb110 NCs are 0.65ms, 0.53 ms and 0.63 ms respectively, as calculated from the decay analysis. The decay curves can be fitted well using the equation $I = A_1 \exp(-t/\tau_1)$ where τ is the lifetime (shown in Fig. S6). The difference in lifetime for the three different NCs can be explained on the basis of their different sizes. With decrease in nanocrystal size, the ions doped in it become more exposed to the high energy vibrational modes of the environment (solvent in this case).

Consequently, the excited states of the dopant ions become more prone to non-radiative relaxation leading to lower luminescence lifetime. As both Pb80 and Pb110 are larger in size than Pb95, the luminescence lifetime of Eu^{3+} ions doped in these NCs is less susceptible to quenching than that observed for Pb95. Quantum yield for all three samples were calculated using quinine sulphate as the reference standard. The quantum efficiency of Pb80, Pb95 and Pb110 were found to be 24.55%, 24.09% and 8.01%, respectively. The details of the measurement and the calculations are given in Fig. S7.

Recently, several studies have investigated the photocatalytic degradation properties of $PbMoO_4$. For this purpose, different synthetic routes have been proposed to obtain new structural morphologies and particle size to improve the photocatalytic efficiency.[27,38-39] As optical absorption property of a material is a key parameter for its photocatalytic activity, diffuse reflectance spectroscopy (DRS) measurements for all three samples were performed. UV-Vis diffuse reflectance spectra of all three Eu^{3+}-doped $PbMoO_4$ NCs show similar reflectance spectra (shown in Fig. 5). Due to the relatively high band gap energy of $PbMoO_4$ (E_g ~ 3.3 eV), it was tested as a photocatalyst under UV irradiation. The conduction band of $PbMoO_4$ is located above the RhB redox potential ($E^0_{RhB^{\bullet+}}$ =1.34 eV) versus the standard calomel electrode (SCE), allowing $PbMoO_4$ to be catalytically active.

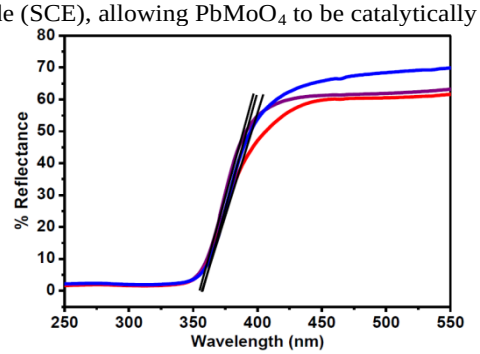

Fig. 5. UV−Vis diffuse reflectance spectra of Eu^{3+} doped Pb80 (blue), Pb95 (red) and Pb110 (violet) nanocrystals.

Upon UV excitation, an exciton is generated in $PbMoO_4$ NCs. The electron in the conduction band and the hole in the valence band reacts with oxygen and water molecules to produce $O_2^{\bullet-}$ and HO•, respectively. We believe that these reactive oxygen species (e.g., HO•, $O_2^{\bullet-}$, etc.) can oxidize the organic dye molecules and perform photocatalysis.[27,40-43] A scheme illustrating the photo-generated charge separation in $PbMoO_4$ NCs and subsequent generation of reactive oxygen species, which is responsible for dye degradation is shown in Fig. 6.

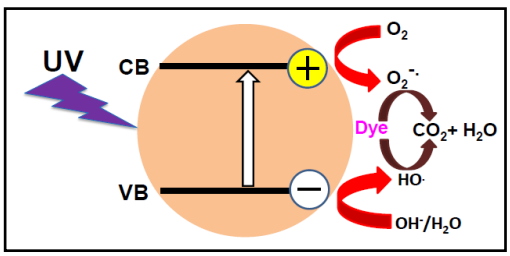

Fig. 6. Scheme depicting photogenarated charge separation and dye degradation by $PbMoO_4$ NCs.

The UV-Vis spectra of RhB (shown in Fig. 7b), collected at regular intervals during the photocatalysis experiment using Pb95 suggests that, the photocatalyst is able to degrade about 70% of RhB dye within 100 minutes of UV irradiation at pH 5.5. Under similar conditions, only 40% of RhB got degraded by TiO_2 (P25) after 100 minutes.

The pie chart diagram of RhB dye degradation shown in Fig. S8 reveals that over half the concentration of the dye is degraded in the first 60 minutes. To quantify the photocatalytic activity of the samples, kinetics of the reactions were investigated. The RhB dye degradation follows apparent first order kinetics, which is in agreement with a general Langmuir–Hinshelwood mechanism;

$$r = -dC/dt = k_1k_2C/(1 + k_2C)$$

where, r is the degradation rate of the dye (mg min^{-1}), C is the concentration of the dye (mg l^{-1}), t is the illumination time, k_2 is the adsorption coefficient of the dye (mg^{-1}), and k_1 is the reaction rate constant (mg min^{-1}). If C is very small then the above equation could be simplified to:

$$\ln(C_0/C) = k_1k_2t = kt$$

where, C_0 is the initial concentration of the dye, C is the concentration of the dye after a certain time *t* with UV illumination, *k* is the rate constant and *t* is the time. The slope of a plot of $\ln(C_0/C)$ vs. *t* (min.) for the dye degradation by the Pb95 NCs (Fig. S9b) provided the rate constant (*k*) (0.010 min^{-1}) of the photocatalytic process. The rate constants of dye degradation by Pb80 and Pb110 were derived in the same way and were found to be similar (as shown in Fig. S9a and S9c, respectively). It is interesting to note here that, contrary to our expectations, there is hardly any role of the nature of the charge present on the photocatalysts' surface for our samples. When Pb80 and Pb110 were used, they showed similar efficiency as photocatalyst (Fig. 7a and 7c). To confirm that Ln^{3+} ions doped in the matrix do not affect the photocatalytic activity of $PbMoO_4$ NCs, control experiments were carried out using undoped $PbMoO_4$ and La^{3+} doped $PbMoO_4$ as photocatalysts. Under similar conditions, both photocatalysts showed similar photocatalytic degradation efficiency (shown in Fig. 7d and 7e, respectively).

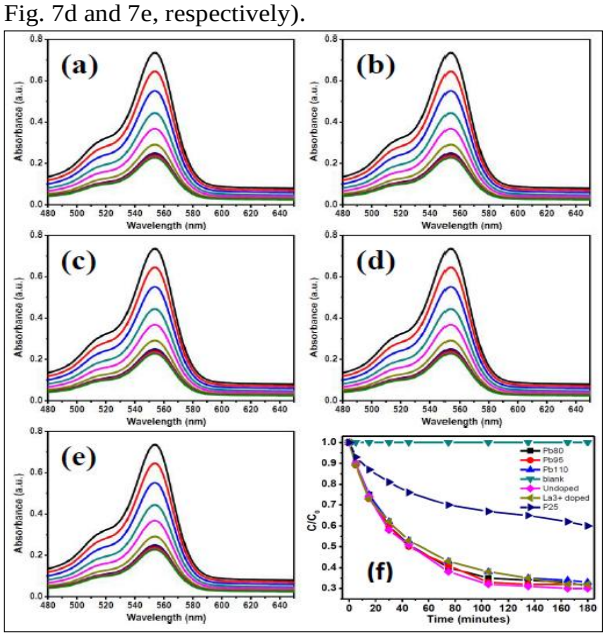

Fig. 7. Temporal evolution of UV−Vis spectra of RhB degradation under visible light in the presence of- (a) Pb80, (b) Pb95, (c) Pb110, (d) Undoped $PbMoO_4$ and (e) La^{3+} doped $PbMoO_4$. (f) shows the concentration change of RhB over time in different photocatalyst solutions.

The Photocatalytic activity of a material largely depends upon its bandgap. However, the DRS results suggest that the observed bandgap values for all the three nanocrystals are quite close (~ 3.3 eV). Although the amount of Pb% affects the size of the nanocrystals, the difference in size between the nanocrystals is quite small (11, 9 and 10.4 nm, respectively for Pb80, Pb95 and Pb110). The observed similar bandgap values for the three nanocrystals are also reflected in the similar photocatalytic behaviour.

To the best of our knowledge, the performance of our photocatalyst surpasses previous reports, both in terms of degradation limit and rate constant at this pH.[41-43] The enhanced photocatalytic activity (at pH 5.5) of our samples in comparison to other reports is illustrated in Table 1 in the ESI. This enhanced photocatalytic activity can be directly attributed to the absence of capping ligands on the surface. The photocatalyst can transfer holes and electrons much more efficiently to oxygen and RhB in the absence of any capping ligands on its surface, thereby producing enhanced photocatalytic activity.

4. Conclusions

We have described here a generic synthetic protocol to prepare ligand-free, all-inorganic NCs that form a colloidal dispersion in polar solvents. The surface of these NCs is designed to have excess residual ions compared to the counter-ionic species, thereby providing a partially charged nanocrystal surface. These charged nanocrystal surfaces cause electrostatic repulsion, providing colloidal stability in polar solvents. SEM measurements suggest that, the average size of the Eu^{3+}- doped $PbMoO_4$ NCs is around 10 nm. Upon UV excitation, aqueous dispersion of Eu^{3+}-doped $PbMoO_4$ NCs show strong red emission, characteristic of Eu^{3+} ions. In addition, due to the absence of any capping agent on their surface, $PbMoO_4$ NCs show strong photocatalytic activity and this is verified from RhB dye degradation under UV illumination. The photocatalytic activity is not influenced by the partial charges present on the surface of the NCs. The strong luminescence, water dispersibility and photocatalytic activity of the Ln^{3+} -doped $PbMoO_4$ NCs provide a platform for their usage as potential candidates in dual applications. We believe, this strategy could be extended to synthesize other colloidal NCs.

Acknowledgements

VM thanks the Department of Science and Technology (DST) India, Council of Scientific and Industrial Research (CSIR) and IISER-Kolkata for the funding. SG and CH thank IISER-Kolkata and TS thanks UGC for their scholarships.

Notes and references

[a] Department of Chemical Sciences, Indian Institute of Science Education and Research (IISER), Kolkata, Mohanpur, West Bengal 741252, India.

Electronic Supplementary Information (ESI) available: [DLS, Zeta potential, EDS, TGA, Lifetime measurement data, Quantum yield calculation, Pie chart diagram, Rate constant determination, Table for comparison of photocatalytic capability between different materials]. See DOI: 10.1039/b000000x/

1 J-C. G. Bünzli and S. V. Eliseeva, *Chem. Sci.*, 2013, **4**, 1939: J-C. G. Bünzli and C. Piguet, *Chem. Rev.*, 2002, **102**, 1897.

2 T. Montini, A. Speghini, L. De Rogatis, B. Lorenzut, M. Bettinelli, M. Graziani and P. Fornasiero, *J. Am. Chem. Soc.*, 2009, **131**, 13155.

3 P. Ptacek, H. Schäfer, O. Zerzouf, K. Kömpe and M. Haase, *Adv. Funct. Mater*. 2007, **17**, 3843.

4 A. M. Cross, P. S. May, F. C. J. M. van Veggel and M. T. Berry, *J. Phys. Chem. C*, 2010, **114**, 14740.

5 P. Ghosh, A. Kar and A. Patra, *J. Appl. Phys.*, 2010, **108**, 113506; A. M. Kaczmarek and R. Van Deun, *Chem. Soc. Rev.*, 2013, 42, 8835.

6 J. Pitchandi, F. C. J. M. Van Veggel and M. Raudsepp, *ACS Appl. Mater. Interfaces*, 2010, 2, 157.

7 P. Harvey, C. Oakland, M. D. Driscoll, S. Hay and L. S. Natrajan, *Dalton Transactions*, 2014, **43**, 5265.

8 M. H. Lee, S. G. Oh, S. C. Yi, D. S. Seo, J. P. Hong, C. O. Kim, Y. K. Yoo and J. S. Yoo, *J. Electrochem. Soc.*, 2000, **147**, 3139.

9 A. Dash, S. Sarkar, V. N. K. B. Adusumalli and V. Mahalingam, *Langmuir*, 2014, **30**, 1401.

10 J. Liu, Q. Yao and Y. Li, *Appl. Phys. Lett.*, 2006, **88**, 173119-1-173119-3.

11 A. J. Steckl, M. Garter, D. S. Lee, J. Heikenfeid and R. Birkhahn, *Appl. Phys. Lett.*, 1999, **75**, 2184.

12 Y. Wang, P. Yang, P. Ma, F. Qu, S. Gai, Y. Dai, N. Niu, F. He and J. Lin, *J. Mater. Chem. B*, 2013, **1**, 2056.

13 A. Leto, F. Piccinelli, G. Pezzotti, A. Speghini, L. Nodari, S. Polizzi, M, Bettinelli, *Materials Research Bulletin*, 2014, **54**, 24.

14 V. Sudarsan, F. C. J. M. Van Veggel, R. A. Herring and M. Raudsepp, *J. Mater. Chem.*, 2005, **15**, 1332; P.R. Diamente, R.D. Burke, F.C.J.M. van Veggel, *Langmuir*, 2006, **22**, 1782; C. Hazra, T.Samanta, and V. Mahalingam, *J. Mter. Chem. C*, 2014, **2**, 10157.

15 A. Nag, M. V. Kovalenko, J. S. Lee, W. Liu, B. Spokoyny and D. V. Talapin, *J. Am. Chem. Soc.*, 2011, **133**, 10612.

16 D. V. Talapin and C. B. Murray, *Science*, 2005, **310**, 86.

17 M. Law, J. M. Luther, O. Song, B. K. Hughes, C. L. Perkins and A. J. Nozik, *J. Am. Chem. Soc.*, 2008, **130**, 5974.

18 M. V. Kovalenko, M. Scheele and D. V. Talapin, *Science*, 2009, **324**, 1417.

19 A. G. Dong, X. C. Ye, J. Chen, Y. J. Kang, T. Gordon, J. M. Kikkawa and C. B. Murray, *J. Am. Chem. Soc.*, 2010, **133**, 998.

20 E. L. Rosen, R. Buonsanti, A. Llordes, A. M. Sawvel, D. J. Milliron and B. A. Helms, *Angew. Chem., Int. Ed.*, 2012, **51**, 684.

21 E. J. W. Verwey, *Chem. Rev.*, 1935, **16**, 363.

22 K. P. Kadlag, M. J. Rao and A. Nag, *J. Phys. Chem. Lett.*, 2013, **4**, 1676.

23 K. Gopalakrishnan, H. M. Joshi, P. Kumar, L. S. Panchakarla, C.N.R. Rao, *Chem Phys Lett.*, 2011, **511**, 304.

24 B. Das, P. Kumar, C. N. R. Rao, *J. Clust. Sci.*, 2012, **23**, 649.

25 D. Piwowarska, S. M. Kaczmarek and M. Berkowski, *J. Non-Cryst. Solids*, 2008, **354**, 4437.

26 M. R. D. Bomio, L. S. Cavalcante, M. A. P. Almeida, R. L. Tranquilin, N. C. Batista, P. S. Pizani, M. Siu Li, J. Andres and E. Longo, *Polyhedron*, 2013, **50**, 532.

27 M. Hashim, C. Hu, X. Wang, X. Li and D. Guo, *Appl. Surf. Sci.*, 2012, **258**, 5858.
28 H. C. Zeng, *J. Mater. Res.*, 1996, **11**, 703.
29 D. B. H. Uresti, J. A. A. Garib and A. M. de la Cruz, *J. Microwave Power E.E.*, 2012, **46(3)**, 163.
30 M. Shen, Q. Zhang, H. Chen and T. Peng, *Cryst. Eng. Comm.*, 2011, **13**, 2785.
31 S. Sarkar, A. Dash and V. Mahalingam, *Chem. Asian J.*, 2014, **9(2)**, 447.
32 Y. Cheng, Y. Wang, D. Chen and F. Bao, *J. Phys. Chem. B*, 2005, **109**, 794.
33 K. Momma and F. Izumi, *J. Appl. Crystallogr.*, 2008, **41**, 653.
34 C. Hazra, T. Samanta, A. V. Asaithambi and V. Mahalingam, *Dalton Trans.*, 2014, **43**, 6623.
35 A. K. Parchur, R. S. Ningthoujam, S. B. Rai, G. C. Okram, R. A. Sing, M. Tyagi, S. C. Gadkari, R. Tewari and R. K. Vatsa, *Dalton Trans.*, 2011, **40**, 7590.
36 N. Yaiphaba, R. S. Ningthoujam, N. S. Singh, R. K. Vatsa, N. R. Singh, S. Dhara, N. L. Misra and R. Tewari, *J. Appl. Phys.*, 2010, **107**, 034301.
37 G. Pan, H. Song, Q. Dai, R. Qin, X. Bai, B. Dong, L. Fan and F. Wang, *J. Appl. Phys.*, 2008, **104**, 084910.
38 G. J. Xing, R. Liu, C. Zhao, Y. L. Li, Y. Wang and G. M. Wu, *Ceram. Int.*, 2011, **37**, 2951.
39 A. M. de la Cruz, D. B. H. Uresti, L. TorresMartínez and S. W. Lee, *React. Kinet. Mech. Catal.*, 2012, **107**, 467.
40 A. Lipovsky, A. Gedanken, Lubart, L. Rachel, *Photomedicine and Laser Surgery*, 2013, **31**, 526.
41 A. M. de la Cruz, D. B. H. Uresti, L. TorresMartínez and S. W. Lee, *React. Kinet. Mech. Catal.*, 2012, **107**, 467.
42 M. R. D. Bomio, R. L. Tranquilin, F. V. Motta, C. A. Paskocimas,; R. M. Nascimento, L. Gracia, J. Andres and E. Longo, *J. Phys. Chem. C*, 2013, **117**, 21382.
43 D. B. H. Uresti, A. M. de la Cruz and L. TorresMartínez, *Res. Chem. Intermed.*, 2012, **38**, 817.

Table of Contents

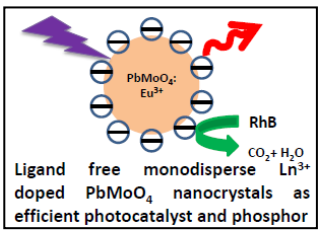

Ligand free monodisperse Ln^{3+} doped $PbMoO_4$ nanocrystals as efficient photocatalyst and phosphor